

## Nusselt number and flow distribution analysis over the roughened surface in a rectangular channel of a solar air heater

Amit Kumar<sup>a\*</sup> and Apurba Layek<sup>b</sup>

<sup>a</sup>"National Institute of Technology Durgapur, Durgapur 713205, India"

<sup>b</sup>" National Institute of Technology Durgapur, Durgapur 713205, India "

\*E-mail: amit4310@rediffmail.com

*Manuscript Received online 6/16/2020, Accepted 9/02/2020*

This paper provides the experimental investigation on the latest development of the optical method primarily based on liquid crystals thermography (LCT) method, which is understood to be a vital tool to obtain surface temperature distribution and assessment of heat transfer coefficients of a rectangular channel using artificial rib roughness. The LCT approach makes use of thermo chromic liquid crystals, an organic material applied at heated surface in an effort to get the color response, which is snapped by a CCD Camera on the premise of temperature modifications. The acquired color sample is digitized and decoded into its HSI (hue, saturation, and intensity) value by the  $R_rG_gB_b$  (red, green, blue) response. The effect of roughness parameters taken into consideration encompasses relative roughness pitch ( $P_i/e$ ) values of 6 - 12, attack angle ( $\alpha$ ) of  $30^\circ$  -  $75^\circ$  and relative roughness width ( $W/w$ ) of 3 - 6 on the improvement of heat transfer are investigated over by varying Reynolds number ( $Re$ ) levels from 13500 - 20500. The objective is to get the Nusselt number variety distribution over the artificially roughened surface with uniform heat flux conditions. It is noted that relative roughness pitch ( $P_i/e$ ) of 8,  $W/w$  of 5 at an attack angle ( $\alpha$ ) of  $60^\circ$  suggests its most beneficial value of heat transfer as compared to smooth absorber surface.

Keywords: Solar air heater, Nusselt number, Winglet ribs, Liquid Cristal Thermography.

### Introduction

The augmentation in heat transfer rate of solar air heater system can be achieved by placing vortex generators of different shapes i.e. circular wire ribs, fins, winglets, obstacle, and perforated blocks between flowing fluid and the heated absorber plate. Generally, the vortex generators have been fabricated to cause interruption as well as the uniform mixing of the flowing fluid in the boundary layer. Nowadays Liquid crystal thermography technique were widely used to formulate the qualitative information regarding temperature distribution using thermo chromic liquid crystals sheet pasted

on the heated surface. It is an optical technique to visualize the effect of temperature distribution through a color response on the heated surface leading to get convective heat transfer coefficient distribution. In the last decade, the number of research work has been made by approaching towards Liquid Crystal Thermography (LCT) technique for various heat transfer applications. Chan et al.<sup>17</sup> did the investigation using LCT approach on oblique/curved surface in order to get the heat transfer distribution. Copper et.al.<sup>5</sup> implemented a problem-based study using LCT technique for augmentation in heat

transfer. Tariq et al.<sup>15</sup> did the LCT based investigation on ribs with a continuous slit which is used to evaluate the Nusselt number distribution. Analysis has been done on different shape vortex generators by Liou et al.<sup>11</sup>, Tanda<sup>14</sup> and Diego Cavallero<sup>4</sup> evaluated the roughness effect on heat transfer as well as pressure penalty in a rectangular duct with roughened rib. Andallib Tariq et al.<sup>16</sup> obtained detailed heat transfer and temperature distribution from flat and roughened surface by using LCT technique. Layek et al.<sup>2</sup> presented an experimental investigation on roughness element comprises of chamfered ribs with groove type roughness in order to get the improvement in heat transfer for the geometrical parameters taken into consideration. Kumar et al.<sup>1</sup> analyse the effect of heat transfer and friction factor phenomenon for twisted ribs roughened surface through the concept of LCT technique. Kumar and Layek<sup>8</sup> did an experimental work on the roughened surface of a solar air heater in order to get the optimal condition of Nusselt number and friction factor using the LCT technique. Kumar and Layek<sup>9, 10</sup> observed through his experimental analysis are that the solar air heater having winglet type roughness on the absorber plate achieve its highest value of heat transfer at  $P_i/e$  of 8,  $\alpha$  of  $60^\circ$  and  $W/w$  of 5 through the concept of LCT technique. The highest enhancement value for Nusselt number and friction factor are recorded to be 2.95 and 2.84 times the smooth channel.

The present investigation deals to analyses the flow visualization for the roughened plate on the basis of surface temperature and the desired effect on heat transfer distribution over the surface, which is

carried out with a different set of geometrical parameters considered. The non-dimensional parameters to define the roughness are relative roughness pitch ( $P_i/e$ ), attack angle ( $\alpha$ ), relative roughness width ( $W/w$ ) and the flow Reynolds number ranges from 13500 - 20500.

## Experimental Procedure

### *Rib Geometry*

For a specific roughness element, the geometry and its shape is considered to be an important factor to achieve its target value on the basis of its operating conditions. Fig.1 depict the schematic sketch diagram of the required winglet ribs used on the absorber surface for the investigation. The positioning and general geometry of the delta winglet type as a rib roughness on the absorber surface are depicted in Fig.2. The non-dimensional parameters are considered and operating range are presented in Table 1. Where 'e' nomenclature as the rib height.

**Table 1.** Operating parameters

Parameters	Ranges			
Relative roughness pitch ( $P_i/e$ )	6	8	10	12
Attack angle ( $\alpha$ )	$30^\circ$	$45^\circ$	$60^\circ$	$75^\circ$
Relative roughness width ( $W/w$ )	3	4	5	6

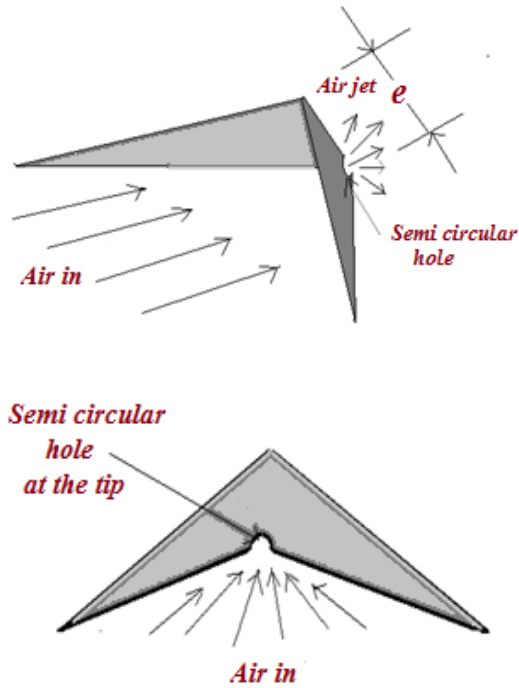


**Fig. 1.** Schematic Sketch diagram of winglet rib

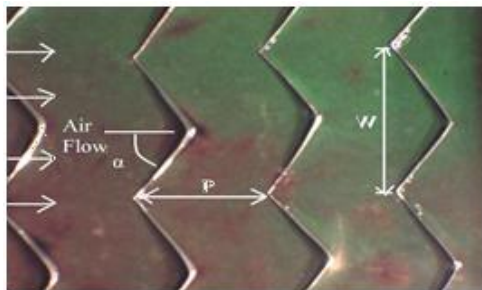


**Fig. 2.** Delta winglet ribs

### Experimental setup details

Fig. 3 represents the schematic sketch diagram of the experimental setup as well as the required instruments utilized in the solar air heater. The experimental setup consists a rectangular channel comprises of three sectional part namely inlet part, test part and exit part which is designed according to ASHARE Standard<sup>3</sup>. In addition to this, the illuminating system, CCD camera and a data logger along with a

computer are also used. The experimentation is done in an open-loop flowing system and the length of the inlet and exit part as per the ASHRAE standard<sup>3</sup> is  $5\sqrt{WH}$  and  $2.5\sqrt{WH}$ . Aluminum plate having a thickness of 3 mm act as a heat transfer surface placed inside the test section with an electric heater to provide uniform heat flux. The radiation effect is only considered for heating the absorber surface and the uniform amount of heat flux given to the absorber surface is absorbed by the radiation process only. T-type thermocouple (24 SWG) is used to record the air temperature for the inlet and exit section. A digital type micro-manometer is installed in a line to measure the pressure drop across the test section. An orifice meter along with a digital differential pressure gauge used to measure the velocity of the flowing fluid or mass flow rate. The photographic image of the experimental setup with its instrumental parts is depicted in Fig.4.

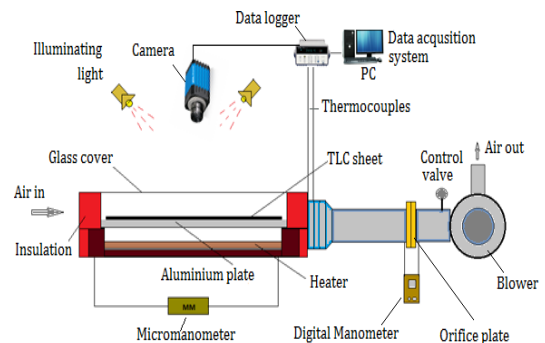


**Fig. 3.** Schematic diagram of an experimental set-up



**Fig.4.** Pictorial view showing experimental Setup

### Image acquisition approach

The perception of the color distribution from the heated surface is captured by a 3CCD Sony camera connected to a computer to perceive the image from TLC (thermo chromic liquid crystal) sheet. An illumination source having 4 white light bulbs (each of 35 W power) has been used over the test zone. IC capture 2.3 software is used for capturing images in jpeg format. The activation of the color through TLC sheet visible only through in which the reflected light enters the CCD camera having a wavelength which splits into three beams and these beams accompanying red, green and blue arrays.

### Image processing

The images which are captured by a camera are digitized in order to obtain its Hue, Saturation and Intensity (HSI) values from the red, green and blue ( $R_r G_g B_b$ ) domain Kakade et al.<sup>7</sup> by Eqs. (1) - (3). As Hue varies widely with the change in temperature compared to other parameters, therefore the variation in Hue is directly related to the surface temperature.

$$R_r = \text{Max}; H = \frac{G_g - B_b}{6(R_r - \min\{R_r, G_g, B_b\})} \quad (1)$$

$$G_g = \text{Max}; H = \frac{2 + B_b - R_r}{6(G_g - \min\{R_r, G_g, B_b\})} \quad (2)$$

$$B_b = \text{Max}; H = \frac{4 + R_r - G_g}{6(G_g - \min\{R_r, G_g, B_b\})} \quad (3)$$

The Saturation (S) values evaluated by

$$S = 1 - \left[ \frac{\text{Min}(R_r, G_g, B_b)}{I} \right] \quad (4)$$

The required Intensity (I) at a particular point obtained by,

$$I = \frac{R_r + G_g + B_b}{3} \quad (5)$$

### Calibration curve for TLC sheet

The calibration of a TLC (thermo chromic liquid crystal) sheet consists of a heated plate where calibration has been done, controllable power supply and an image capturing system. A pre-packaged (R40C5W) TLC sheet is used for the visualization of temperature on the organic crystal materials which is used to get the color response in a reversible and repeatable pattern as the temperature changes. During the calibration process proper care and attention was taken in order to prevent interference from the surroundings light noise. The colorless image i.e. black color appears till it reaches the active temperature, it turns red, green and blue sequentially again turns to colorless when the temperature exceeds its active ranges. The color-temperature play interval depends on the TLC composition

Stasieka et al.<sup>13</sup>.

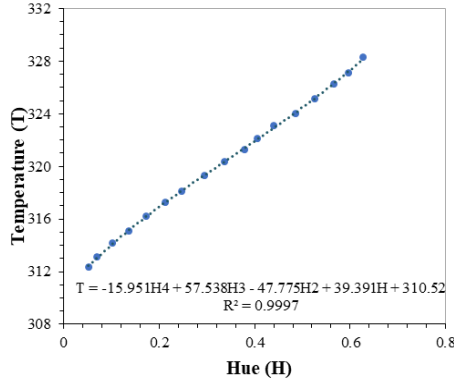


**Fig. 5.** Calibration curve for TLC sheet  
The calibration curve plotted for the hue-temperature relationship is shown in Fig. 5 and the relation obtained between Temperature and hue is given by Eq. (6)

$$T = -15.951 H^4 + 57.538 H^3 - 47.775 H^2 + 39.391 H + 310.52 \quad (6)$$

#### Data Reduction

As the surface of the plate reached to steady state condition, the recorded TLC image which captured through a CCD camera are transformed it into a bmp files using frame grabber. The R<sub>r</sub>G<sub>g</sub>B<sub>b</sub> value of the sample images changes to that with HSI values only through pixel by pixel using the MATLAB software code. The TLC image obtained has been digitized to its hue values and these hue values thus used to calculate wall temperature to calculate convective heat transfer coefficient ( $h$ ) given by using following relationship.

$$h = \frac{Q}{(T_{LCT} - T_{fm})} \quad (7)$$

Where, Q noted as convective heat flux,  $T_{LCT}$  given in Eq. (7) known to be heated plate temperature through the color output of the

TLC sheet and  $T_{fm}$  is mean fluid temperature for the given x- position. For the given x-distance the following relation has been used to measure the mean fluid temperature of the flowing fluid.

$$T_{fm} = T_i + \frac{Q_{conv} A_p (x/L)}{mC_p} \quad (8)$$

The required value of Nusselt number (Nu) and Reynolds number (Re) thus used are given by using following relationship.

$$Nu = \frac{hD_h}{k} \quad (9)$$

$$Re = \frac{VD_h}{\nu} \quad (10)$$

Fig. 6. depicts the LCT captured image over the smooth plate showing its R<sub>r</sub>G<sub>g</sub>B<sub>b</sub> (Red, Green and Blue) values. In order to get the accuracy of the measurement the set up validation has been conducted for a smooth channel to obtain Nusselt number (Nu) as shown in Fig.7 and the data which is obtained from the experimentation is used for the comparison with Dittus-Boelter Equation McAdams<sup>12</sup> given by Eq.(11).

Dittus-Boelter Equation:

$$Nu_s = 0.023 Re^{0.8} Pr^{0.4} \quad (11)$$

The Nusselt number ( $Nu_s$ ) deviation with the empirical relation for the smooth surface under fully developed flows condition deviated by 2.76 %.

#### Experimental Uncertainty

The error encountered mainly due to some experimental uncertainty in the observed data which is suggested by Coleman and Steele<sup>6</sup>. The required uncertainty value recorded for (Nu) and (Re)

at the 95% confidence level is noted to be of 3.69 and 3.82 % respectively for  $Re=13500$  and similarly, those for  $Re=20500$  are 4.21 and 2.92 % respectively.

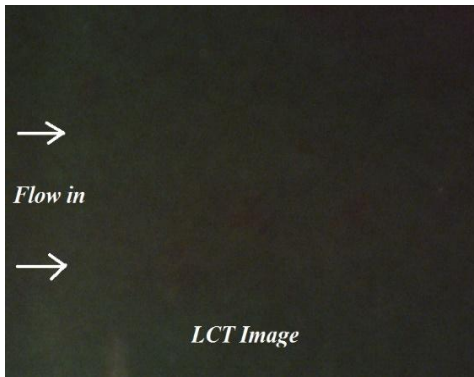


**Fig. 6.** LCT captured image over the smooth plate showing its  $R, G, B_b$  (Red, Green and Blue) values

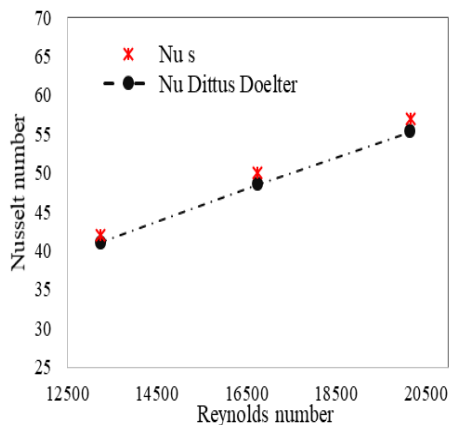


**Fig. 7.** Nusselt number Vs Reynolds number for the smooth surface

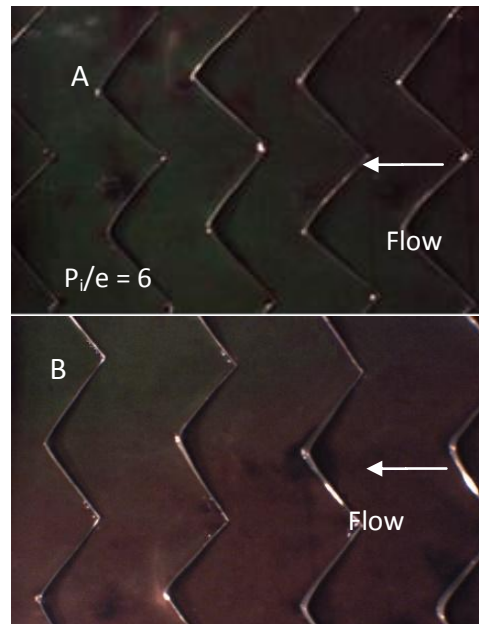
## Results and discussion

### Effect of relative roughness pitch

As depicted in Fig. 8, the roughness element was embedded on the heated side of the test surface in order to visualize the characteristics of temperature distribution using the Liquid crystal optical system for the geometric arrangements at

an angle of attack  $60^\circ$ , relative roughness width of 5 and varying relative roughness pitch of 6, 8, 10 and 12. The image thus obtained through LCT sheet has been used to get the local value of heat transfer coefficient.

For relative roughness pitch of 6, flow reattachment at the consecutive ribs does not takes place in the inter-rib region as seen from Fig 8 appears to be of green color due to its higher plate temperature. Further, increasing the  $P/e$  values to 8, red color appears between the inter-ribs and that region shows that the reattachment is possible. Further increase of  $P/e$  value to 10-12, the color response that appears gradually decreases and increases to the high intensity of green color, which clearly indicates that the flow reattachment between the ribs is supposed to be less than





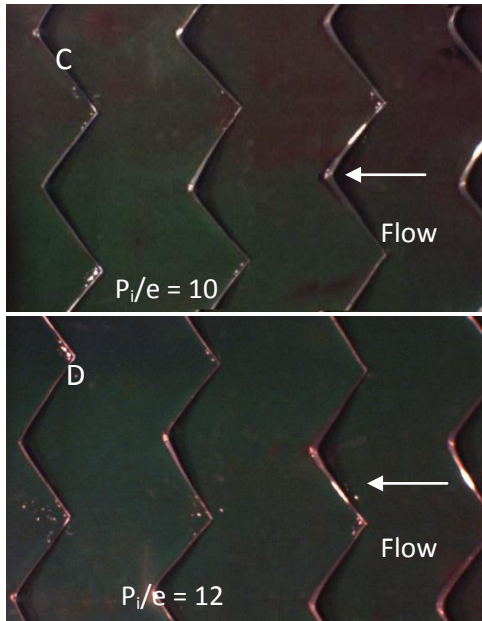


**Fig. 8.** LCT captured image at Re 20500 for  $P_i/e = 6, 8, 10, 12$

the previous arrangement. As presented in Fig 9, it clearly shows that the Nusselt number is found to be less at  $P_i/e$  of 6, and attain its maximum values at  $P_i/e$  of 8 for all values of Reynolds number.

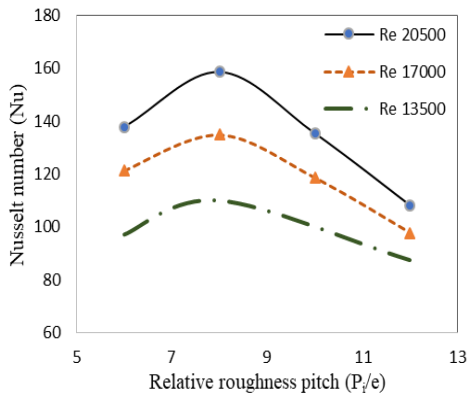


**Fig. 9.** Effect of relative roughness pitch

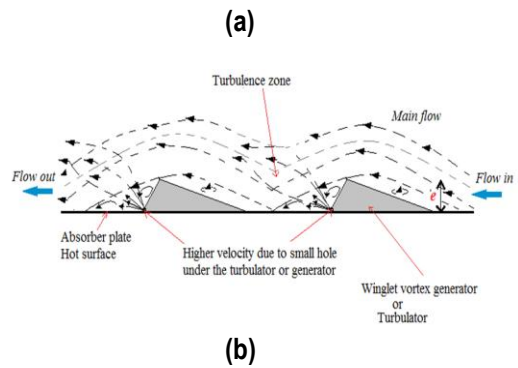
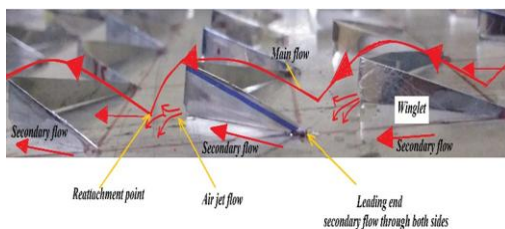


**Fig. 10 (a) and (b)** Pictorial and sketch view showing flow pattern anticipation

The approximate flow pattern using a thin winglet type turbulator geometry with a small hole at the tip of the ribs produces formation of air-jet underside of the absorber surface as depicted in Fig.10 (a) and (b) could definitely prevent the formation of wakes just beside the ribs in the flowing stream and also creates the redevelopment of secondary flow through the leading ends of the ribs. In the present case, provision of the winglet shaped rib on the absorber surface is advantageous in many aspects as it reduces the thermal resistance generated by the presence of viscous sub layer just adjacent to the heated wall which minimises the eddies or wake formation towards the flowing stream and behind the ribs.

### Effect of attack angle

The winglet is arranged on the basis of angle of attack of  $30^\circ, 45^\circ, 60^\circ,$  and  $75^\circ$  as shown in Fig 11, having a constant value of  $P_i/e$  of 8 and  $W/w$  of 5 to observe the temperature distribution in between inter-rib region. It can be seen from the Fig 11 that for attack angle of  $30^\circ, 45^\circ$  and  $75^\circ$  arrangement inter-rib space consists of green color respectively resulting higher value of plate temperature. At  $60^\circ$  angle of

attack temperature distribution is shown (Fig 11 G), appears high intensity of red color mainly due to flow reattachment found to be high. The effect of attack angle on Nusselt number is depicted in Fig 12, it is observed that the maximum Nusselt number attains at angle of attack of 60°.

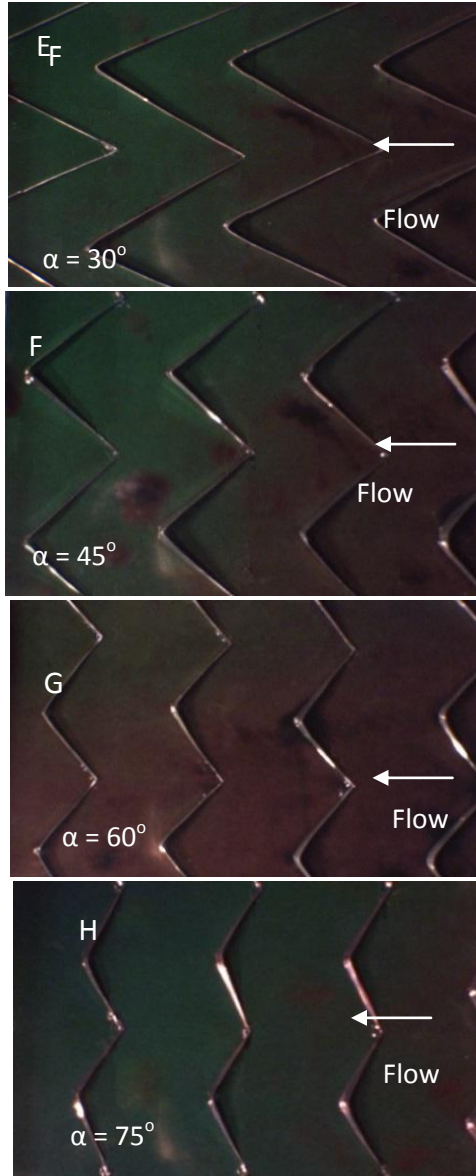


Fig. 11. LCT images captured at re 20500 for

angle of attack ( $\alpha$ ) of 30°, 45°, 60°, 75°.

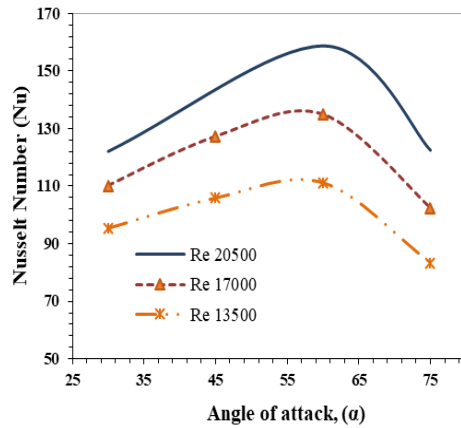
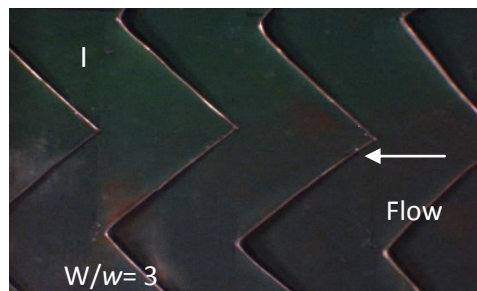


Fig. 12. Effect of attack angle ( $\alpha$ )

#### Effect of relative roughness width

Fig 13, shows the temperature distribution based on LCT study for the surface arrangements of  $\alpha = 60^\circ$ ,  $P/e = 8$  and at varying relative roughness width of 3, 4, 5 and 6. It can be seen from Fig 13, K for  $W/w$  of 5, the high intensity of red color appears on the surface, mainly due to flow reattachment at different location supposed to be high. For arrangement of  $W/w$  of 3, 4 and 6, such images (Fig 13, I, J and L) appears high intensity of green color, indicates that the flow reattachment does occur properly of the free shear layer. Fig 14, shows the effect of relative roughness width on Nusselt number, it can be observed that at  $W/w$  of 3 the Nusselt number is low leads to an optimum value of Nusselt number at  $W/w$  of 5 for all the values of Reynolds number and again decreases for further increase in  $W/w$  values.





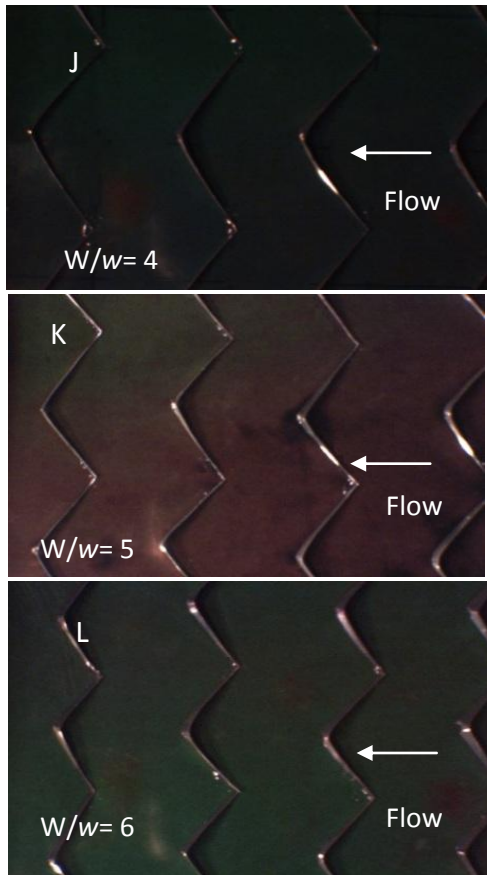


Fig. 13. LCT images captured at re 20500 for relative roughness width of 3, 4, 5, 6.

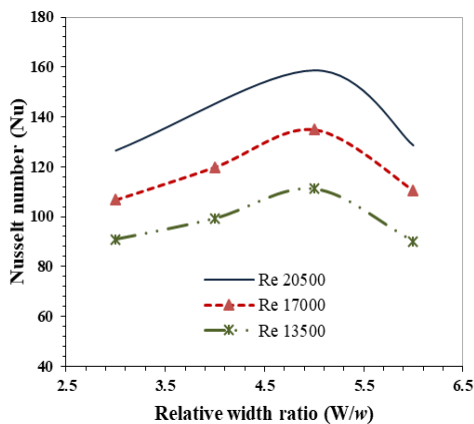


Fig. 14. Effect of relative roughness width (W/w)

### Conclusions

The results showed that the application of LCT technique can provide the temperature

distribution over a surface and are utilized to evaluate the local heat transfer coefficient in order to get further information about the flow field. The zone of reattachment point, vortex generated can be observed over a surface based on the application of LCT technique. A systematic study has been made for different configurations of winglet type rib geometries for evaluating the heat transfer distribution over the heated surface. Based on the present investigation the optimum values of heat transfer coefficient is seen at  $P_i/e$  of 8,  $W/w$  of 5 and  $\alpha$  of  $60^\circ$ . Thus, the heat transfer measurement on the basis of its temperature distribution are strongly recommended to understand the detailed information regarding flow visualization.

### Acknowledgements

The research work was funded by the SERB, DST, Govt. of India, Ref no.: SB/EMEQ 314/2013; dated: 08/07/2013.

### Nomenclature

$A_p$	Absorber surface area, $m^2$
$C_p$	Specific heat (air), J/kg K
$h$	heat transfer coefficient. ( $W/m^2K$ )
$L$	Length of absorber plate, m
$T_{LCT}$	TLC sheet temperature (K)
$T_{fm}$	Mean fluid temperature (K)
$Q$	heat flux (watt)
$Nu$	Nusselt number
$k$	Air thermal conductivity ( $W/mK$ )
$m$	Mass flow rate, kg/s
$V$	Wind velocity of air (m/s)
$Re$	Reynolds number
$\nu$	kinematic viscosity( $m^2/s$ )
$T$	Temperature ( $^\circ C$ )
$H$	Hue
$D_h$	Hydraulic diameter (m)

R,G <sub>9</sub> B <sub>b</sub>	Red, green and blue
W/w	Relative roughness width
P/e	Relative roughness pitch

### **Greek symbol**

$\alpha$	Angle of attack
$\nu$	Air Kinematic viscosity
$\mu$	Fluid Dynamic viscosity
$\rho$	Air Density

### **Subscript**

r	roughened surface
s	smooth surface

### **References**

1. A. Kumar, A. Layek, Nusselt number-friction characteristic for a twisted rib roughened rectangular duct using liquid crystal thermography. *Experimental Thermal and Fluid Science*, 2018, 97, 205–217.
2. A. Layek, J.S. Saini, S.C. Solanki, Effect of chamfering on heat transfer and friction characteristics of solar air heater having absorber plate roughened with compound tabulators, *Renew. Energy*, 2009, 34, 1292-1298.
3. ASHRAE Standards (93-77) Methods of testing to determine the thermal performance of solar collectors, New York.
4. Cavallero, D., Tanda, G., An experimental investigation of forced convection heat transfer in channels with rib turbulators by means of liquid crystal thermography, *Experimental Thermal and Fluid Science*, 2002, 26, pp. 115–121.
5. Copper, T.E., Filed, R.J. and Meyer, J.F. Liquid crystal thermography and its application to the study of convective heat transfer, *transactions of the ASME*, 1975, pp 442-450.
6. H.W. Coleman, W.G. Steele, *Experimentation and Uncertainty Analysis for Engineers*, second Ed. John Wiley & Sons, New York, 1999.
7. Kakade VU, Lock GD, Wilson M, Owen JM, Mayhew JE. Accurate heat transfer measurements using thermo chromic liquid crystal. Part 1: Calibration and characteristics of crystals. *International Journal of Heat and Fluid Flow*. 2009,30,939-49.
8. Kumar A, Layek A. Nusselt number and fluid flow analysis of solar air heater having transverse circular rib roughness on absorber plate using LCT and computational Technique. *Thermal Science and Engineering Progress*. 2019, 14,100398.
9. Kumar A, Layek A. Nusselt number and friction factor correlation of solar air heater having winglet type vortex generator over absorber plate. *Solar Energy*. 2020, 205,334-348.
10. Kumar A, Layek A. Nusselt number and friction characteristics of a solar air heater that has a winglet type vortex generator in the absorber surface. *Experimental Thermal and Fluid Science*. 2020; 23:110204.
11. Liou, T.M, Chen, C.C., Tsai, T.W., Heat transfer and fluid flow in a square duct with 12 different shaped vortex generators, *Journal of heat transfer*,2000,122, pp 327-335.
12. McAdams, W.H., *Heat Transmission*. Mc Graw-Hill, New York, 1942.
13. Stasieka, J., Stasieka, A., Jewartowska, M., and Collins, M.W. Liquid crystal thermography and true-colour digital image processing”, *Optics & Laser Technology*, 2006, 38 pp.243–256.
14. Tanda, G., Heat transfer and pressure drop in a rectangular channel with diamond shaped elements, *International Journal Heat and Mass Transfer*, 2001,44, pp. 3529-3541.
15. Tariq A, Panigrahi P.K., Muralidhar K., Flow and heat transfer in the wake of a surface-mounted rib with a slit. *Experiments in Fluids (Germany)* 2004, 37,701-719.
16. Tariq, A., Swain, S.K., Panigrahi, P.K., An experimental study of convective heat

transfer from flat and ribbed surface,  
Indian journal of engineering and material  
science,2002, 9, pp 464-471.

17. T.L. Chan, K. Jambunathan, T.P. Leung, A  
surface temperature calibration method for  
thermo chromic liquid crystals using true-  
colour image processing, Proceedings of  
the 10th International Heat transfer  
conference, Brighton, UK,14-18 August  
1994, Vol.2, pp.201-206.